Title

Cathepsin B knockout confers significant brain protection in the mouse model of stroke

Authors

Hu, Kurt
Park, Yujung
Olivas, Yamileck
et al.

Publication Date

2023-10-01

DOI

10.1016/j.expneurol.2023.114499

Peer reviewed

Experimental Neurology 368 (2023) 114499

Contents lists available at ScienceDirect

Experimental Neurology

journal homepage: www.elsevier.com/locate/yexnr

Research paper

Cathepsin B knockout confers significant brain protection in the mouse model of stroke

Kurt Hu [a,1], Yujung Park [b,1], Yamileck Olivas [b], Alice Chen [b], Chunli Liu [b], Bingren Hu [b,c,*]

[a] Department of Medicine, Division of Pulmonary and Critical Care Medicine, Medical College of Wisconsin, Milwaukee, WI, United States of America
[b] Departments of Emergency Medicine and Neurosciences, University of California San Diego, La Jolla, CA, United States of America
[c] Veterans Affairs San Diego Healthcare System, 3350 La Jolla Village Dr, San Diego, CA, United States of America

ARTICLE INFO

Keywords:
Mouse stroke
MCAO
Cathepsin B knockout
Behavior performance
Infarct
And histopathology

ABSTRACT

Background: Significant advances have been made in our understanding of the endolysosomal cycle. Disruption of this cycle leads to cell death. The objective of this study aims to investigate the role of disrupted endolysosomal cycle in brain ischemia-reperfusion injury.
Methods: A total of 57 mice were randomly assigned into four experimental groups: (i) wildtype (wt) sham control; (ii) wt middle cerebral artery occlusion (MCAO); (iii) cathepsin B (CTSB) knockout (KO) sham control; and (iv) CTSB KO MCAO. Mice were subjected either to 0 min (sham) or 40 min of MCAO, followed by reperfusion for 1 or 7 days. Physical and behavioral examinations were conducted in the 7-day reperfusion group for 7 consecutive days after MCAO. Confocal microscopy was used to assess the levels, redistributions, and co-localizations of key endolysosomal cycle-related proteins. Histopathology was examined by light microscopy.
Results: Confocal microscopy revealed a significant accumulation of CTSB in post-ischemic penumbral neurons relative to those in the sham group. In addition, N-ethylmaleimide sensitive factor ATPase (NSF) was irreversibly depleted in these neurons. Furthermore, CTSB-immunostained structures were enlarged and diffusely distributed in both the cytoplasm and extracellular space, indicating the release of CTSB from post-ischemic neurons. Compared to wt mice, CTSB KO mice showed a significant decrease in hippocampal injury area, a significant increase in the number of survival neurons in the striatal core area, and a significant improvement in physical and functional performance in post-MCAO mice.
Conclusion: Brain ischemia leads to a cascade of events leading to inactivation of NSF, disruption of the endolysosomal cycle, endolysosomal structural buildup and damage, and the release of CTSB, eventually resulting in brain ischemia reperfusion injury. CTSB KO in mice protected the brain from ischemia-reperfusion injury.

1. Introduction

In mouse stroke models, the most consistent pattern of brain injury following middle cerebral artery occlusion (MCAO) is a time-dependent progression of histopathological damage. This progression includes early infarction in the dense ischemic core within 1–12 h, followed by delayed neuronal death in the lesser ischemic penumbra over 12–72 h after MCAO (Liu et al., 2009). After 24 h post-MCAO, activation of microglia, infiltration of monocyte/neutrophil, and astrogliosis are observed in the brain damage areas (Liu et al., 2009; Fifield and Vanderluit, 2020).

Lysosomes, once described as general digestive organelles, are now recognized as dynamic and continuous groups of structures that constitute the endolysosomal system (de Duve, 2005; Bright et al., 2016). Each structure in this system contains common structural "lysosome" proteins and "lysosome" digestive enzymes, such as acidic proteases known as cathepsins. These structures perform cellular sensing and digestive functions (Bright et al., 2016; Repnik et al., 2013; Winckler et al., 2018; de Araujo et al., 2020; Wang et al., 2018; Papadopoulos et al., 2020). This endolysosomal system comprises three basic

Abbreviations: CTSB, cathepsin B; EL, endolysosome; IRI, ischemia reperfusion injury; KO, knockout; L, lysosome; LE, late endosome; MCA, middle cerebral artery; MCAO, middle cerebral artery occlusion; NSF, N-ethylmaleimide sensitive factor ATPase; SNAP, soluble NSF attachment protein; SNAREs, SNAP receptors.

* Corresponding author at: University of California San Diego, la Jolla, CA 92093, United States of America.
E-mail addresses: kuhu@mcw.edu (K. Hu), yolivasgarcia@ucsd.edu (Y. Olivas), alc022@ucsd.edu (A. Chen), chl216@ucsd.edu (C. Liu), bih001@ucsd.edu (B. Hu).

[1] Co-first authors who contribute equally to the study.

https://doi.org/10.1016/j.expneurol.2023.114499
Received 31 May 2023; Received in revised form 5 July 2023; Accepted 25 July 2023
Available online 26 July 2023

groups of structures: (i) late endosome (**LE**), (ii) endolysosome (**EL),** and (iii) "terminal" lysosome, hereafter referred to as lysosome (**L**). Each group of these structures undergoes a series of transitions from an early naive stage to a mature form (Hu et al., 2021). The LE receives newly synthesized lysosome structural proteins and digestive enzymes from Golgi apparatus as well as waste cargoes from both endocytic and autophagic pathways. However, at its high intraluminal pH (6.0), LE's acidic hydrolases are mostly inactive and cannot degrade the waste cargoes. To process these cargoes, the LE must fuse with a more acidic L (pH 4.0–4.5) to form a hybrid EL (~pH 4.5) (Bright et al., 2016; de Araujo et al., 2020; Bissig et al., 2017; Hu et al., 2021).

The fusion between L and LE is mediated by several protein complexes. The core complex consists of: (i) N-ethylmaleimide sensitive factor ATPase (NSF), (ii) soluble NSF attachment protein (SNAP), and (iii) SNAP receptors (SNAREs) (Hu et al., 2021). Interactions between SNAREs from L and LE membranes facilitate the merging of these two organelles into a single EL. After fusion, SNAREs on the EL membrane form an inactive stable cis-complex that must be dissociated or reactivated by NSF ATPase and its adaptor protein SNAP to convert the EL to a new L. This transitional process, from L-to-LE fusion and then the EL-to-L conversion, is defined as a "endolysosomal cycle". This cycle is crucial for the removal of intracellular protein aggregates and damaged organelles (Hu et al., 2021). While there are >60 members of SNAREs and three members of SNAPs, there is only one member of NSF in mammalian cells (Hong and Lev, 2014; Yoon and Munson, 2018; Baker and Hughson, 2016). Therefore, NSF is a "limiting factor" for the endolysosomal cycle (Hu et al., 2021).

Stroke inactivates NSF, thus disrupting the endolysosomal cycle and leading to blockages in the endocytic and autophagic pathways (Hu et al., 2021; Yuan et al., 2021). This blockage results in damage to the endolysosomal compartments and a large-scale release of cathepsin B (CTSB) into the cytoplasm and extracellular space (Hu et al., 2021; Yuan et al., 2021). There are at least 15 cathepsins distributed in the endolysosomal structures of different organs. Among them, CTSB exhibits endopeptidase activity at a neutral pH and is commonly implicated in cell death (Buck et al., 1992; Cavallo-Medved et al., 2011; Serrano-Puebla and Boya, 2016; Wouters and Bunt, 2016). Furthermore, CTSB is one of the most abundant cathepsins in neurons (Petanceska et al., 1994).

In this study, we utilized CTSB knockout (KO) mice and their corresponding wildtype (wt) mice to explore the role of CTSB in brain ischemia-reperfusion injury, using a mouse MCAO model.

2. Materials and methods

A detailed descriptions of Materials and Methods were included in the supplementary materials.

2.1. Ethics statement

The animal protocols were approved by The Institutional Animal Care and Use Committee (IACUC) at University of California San Diego.

2.2. Animals

Male CTSB KO mice (B6;129-Ctsbtm1Jde/J) and wildtype (wt) control mice (B6;129) at about 3 months of age were used. The breeding pairs of B6;129-Ctsbtm1Jde/J and (B6;129) wt control mice were purchased from Jackson Laboratory (Bar Harbor, ME, USA). Animals were given food and water ad libitum and kept on a 12 h light/dark cycle in climate-controlled housing. They were bred, housed, and cared for in the animal facility according to the institutional guidelines.

2.3. Mouse MCAO model

On the day of surgery, mouse body weight, rectal temperature, surgical procedures, and anesthesia status were documented. Aseptic survival surgical procedures were performed throughout the experiment. Mice were subjected either a sham surgery (0 min ischemia) or 40 min MCAO followed by a 1- and 7-day reperfusion, respectively, using the method as described in our previous study (Yuan et al., 2018a). Briefly, the middle cerebral artery blood flow was monitored via a small incision to affix a needle laser Doppler flowmetry (LDF) probe (MNP100XP, ADInstruments, CO, USA) to the temporal bone surface (Fig. 1A). Via a midline incision in the neck area, the right common carotid artery (CCA), external carotid artery (ECA), and internal carotid artery (ICA) were carefully separated under a surgical microscope. The CCA and ICA were temporarily clamped using a microvascular clip (Fig. 1A). A 12 mm sterilized monofilament (6–0, Nylon suture, United States Surgical, Norwalk, CT, USA) with a silicone-coated tip measuring 0.22–0.23 mm in diameter and 2.0 ± 0.2 mm in length (Supplemental Fig. 1), was carefully introduced into the ECA and further advanced into the ICA (Fig. 1A). From this time point onwards, the LDF probe was affixed to the temporal bone surface directly without a holder and MCA blood flow was continuously monitored for the entire peri-MCAO periods (Fig. 1A). After securing the LDF probe recording, the already inserted monofilament occluder was gently and gradually advanced to the base of MCA without disturbing the LDF probe. The monofilament occluder was determined to have reached the MCA base when MCA blood flow dropped sharply to below 10% of the pre-ischemic level (Fig. 1B). After 40 min MCAO, the monofilament occluder was removed to start reperfusion (Fig. 1B). After a reperfusion period of 15–20 min, isoflurane was discontinued, and all wounds were sutured. The mouse was returned to its home cage for post-stroke care. The sham-operated mice received the same surgical procedures, with the exception that the monofilament was inserted through the ECA to the ICA but not further advanced into the base of MCA. All mice post-stroke were kept in a controlled temperature environment using the Solace Zone set at 80 °F (Solace Inc., MI, USA). Additionally, each mouse received a daily subcutaneous administration of 0.5 ml per 25 g bodyweight of sterile Ringer's solution for 5 consecutive days.

2.4. Experimental group

A power analysis based on our pilot data (power 0.80, alpha 0.05, and beta 0.2) showed that: (i) >8 mice per group were required for the behavioral and histopathological analysis and (ii) >3 mice per group were required for the confocal analysis. Experimental groups were: (i) wt sham followed by 1 day (for confocal, $n = 5$) and 7 days (for histopathology, $n = 8$) of reperfusion; (ii) CTSB KO sham at 1 day (n = 5) and 7 days (n = 8) of reperfusion; (iii) wt 40 min MCAO at 1 day (n = 5) and 7 days of reperfusion (n = 8); and (iv) CTSB KO 40 min MCAO at 1 day (n = 5) and 7 days of reperfusion ($n = 13$). For confocal microscopy, mice were perfusion-fixed with 4% paraformaldehyde at 1 day of reperfusion. For behavioral and physical evaluations, mice underwent nest building activity test, pole test, and body weight exam. At the 7-day endpoint, mice were perfusion-fixed with 4% paraformaldehyde for histopathological analysis.

2.5. Survival rate and mortality

Subject death time and possible etiology were documented during the day by investigators and during the night (between 1700 and 0930) using the PhenoTyper infrared video device and its software (Noldus, VA, USA). During the night, mice were continuously monitored through video surveillance, and mice showing no breathing or movement for 1 h were considered dead. The death was confirmed in the following morning by investigators.

2.6. Body weight

Mice were weighed at about 5 min before surgery and then daily at

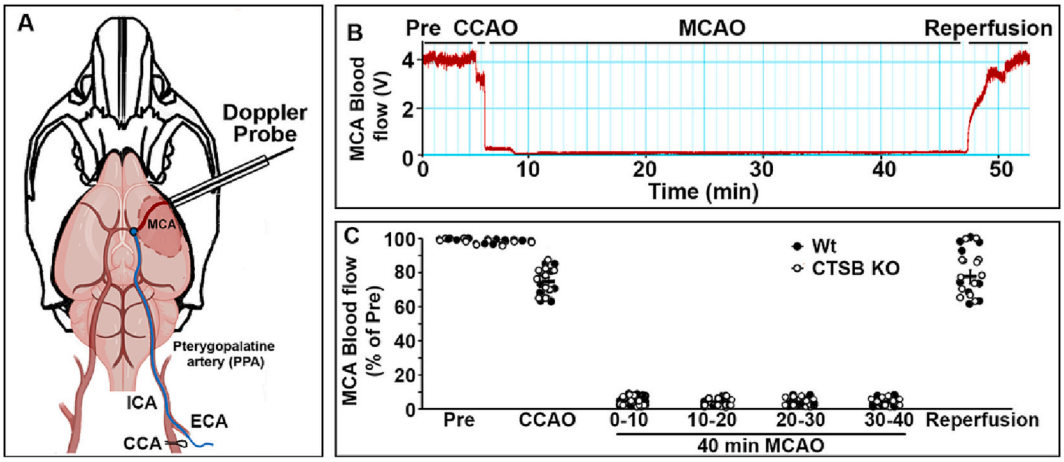

Fig. 1. *A: Schematic middle cerebral artery (MCA) occlusion (MCAO) procedures.* A Laser Doppler Probe was affixed to the exposed temporal bone surface to record the MCA blood flow during the entire peri-MCAO periods. A monofilament occluder was inserted via an incision of the external carotid artery (ECA), gone through the internal carotid artery (ICA), and advanced to the base of the MCA. *B:* An example of Laser Doppler Flowmetry of the blood flow in the MCA region. The MCA blood flow was reduced: (i) by 20–50% after temporary clamping of the common carotid artery (CCAO), and (ii) by >90% after MCAO. After monofilament removal, MCA blood flow returns to above 60% of pre-ischemic level, which was used as a confirmation of reperfusion. *C:* The MCA blood flow was continuously monitored during the peri-MCAO periods in all mice used in this study.

around 10:00 AM until reaching the endpoint. The measurement was performed in a double-blind manner.

2.7. Nest building activity

Mice were individually housed with normal corn cob-chip bedding without environmental enrichment items. The nest-building activity was documented daily according to our previous study with modifications (Yuan et al., 2018a). Briefly, three 5 cm square pieces of pressed cotton nestlets were placed in each cage at 10 AM. The following day, at 10 AM, the maximal amounts of torn and untorn nestlet materials in each cage were weighed. Untorn pieces were defined as those that were weighed >0.05 g. The percentage of torn nestlet materials to untorn materials were calculated. Mice were tested in a double-blind manner on the day before surgery and daily following surgery.

2.8. Pole test

A 90 cm vertical steel pole with a diameter of 10 mm was uniformly wrapped with tape and placed in a testing box (e.g., an empty mouse cage). Two layers of a bubble wrap pad covered with a blue pad were placed on the floor of the testing box to provide cushioning. After adapting to the testing box environment for 2 min, the mouse was positioned head downward on the pole with its forelimbs placed at the 60 cm line above ground. The total time for the mouse to walk to the ground floor (defined as all four limbs leaving the pole) was recorded with a stopwatch. Mice were pre-trained three times prior to the formal test in the same manner and were rested for 30 s between trials. For each mouse, a total of three runs were performed and the average time to reach the ground was calculated. If mice fell immediately from the 60 cm line to the ground, a total time equal to the longest time in the group was given. The mouse had to walk down continuously without pause, otherwise the test was cancelled and repeated. If the mouse slid down from the pole, a total time equal to the longest time in the group was given. Mice were tested in a double-blind manner on 1-, 3-, and 7-day after the surgery, respectively.

2.9. Confocal microscopy

Double-immunolabeling fluorescence confocal microscopy was performed using coronal brain sections (50 μm) in a double-blind manner according to the method described in our previous studies (Yuan et al., 2018b; Yuan et al., 2018c). Brain sections were double-labeled with the following pairs of antibodies: (i) CTSB and Iba-1, (ii) CTSB and NeuN, and (iii) NSF and CTSB. The antibody species reactivity and usage information are provided in Supplemental Table 1. The fluorescence intensity of images taken with the Zeiss laser-scanning confocal microscope was measured with ImageJ in the ipsilateral and contralateral areas of post-MCAO and sham brains. The details of the quality control of confocal microscopy and quantification of confocal microscopic fluorescence intensity were provided in the Supplementary Materials and Methods.

2.10. Quantitative histopathological analysis

The size of the brain damage was quantitatively assessed in a double-blind manner using the same method described in our recent publications (Yuan et al., 2018a) and detailed in the Supplementary Materials and Methods. Hematoxylin and eosin (H&E) staining was performed on brain sections. The average damage sizes were analyzed at the striatal (0.50 mm to Bregma) and dorsal hippocampal (−1.82 mm to Bregma). To ensure consistency among different subjects, the size and location of the lateral ventricle, medial septal nuclei, and anterior commissure were used as landmarks for identifying brain sections at the striatal level. Similarly, the dorsal third ventricle and lateral ventricle were used as landmarks to identify the dorsal hippocampal sections. The percentage of the ipsilateral damage area was calculated based on the difference between the undamaged contralateral area and the undamaged ipsilateral area using a formula; (undamaged contralateral area – undamaged ipsilateral area)/(undamaged contralateral area) x 100. Furthermore, the average number of surviving neurons within one cubic millimeter volume in the center of the striatal ischemic core was counted in a double-blind manner. Quantitative analysis was performed on every tenth 50 um-thick H&*E*-stained section of the striatum between 1.35 and 0.35 mm (3 sections) posterior to the Bregma, using the SteroInvestigator program (MBF Biosciences, VA, USA) based on the unbiased stereological principle.

2.11. Statistics and analysis

Statistical analysis was conducted using KaleidaGraph software (Synergy Software, PA, USA). A two-tailed *t*-test was used to analyze the data from two experimental groups. One-way ANOVA followed by Tukey's test was used to analyze data from more than two experimental

groups. The Wilcoxon-Mann-Whitney Test (2*1 sided exact) was utilized for statistical analysis of behavioral performance. Data are presented as means ± SEM, and a p-value <0.05 was considered statistical significance.

3. Results

3.1. Vigor and reproducibility

Continuous monitoring of MCA blood flow is essential to ensure adequate ischemia and reperfusion in this mouse model (Fig. 1) (Yuan et al., 2018a). Ischemic stroke was confirmed when the average MCA blood flow level fell under 10% of the pre-ischemia level during the entire MCAO period (Fig. 1, A-B). Reperfusion was confirmed when the blood flow returns to >65% of the pre-ischemia level within 15–20 min of reperfusion (Fig. 1, A-B). In this study, the MCA blood flow was continuously monitored, and ischemic and reperfusion levels were successfully achieved in every mouse (Fig. 1C).

3.2. Massive buildup of CTSB primarily in post-ischemic penumbral neurons

To study the cellular distribution of CTSB, we double-labeled 24-h post-MCAO brain sections with CTSB and Iba-1 antibodies (Fig. 2). In the ipsilateral striatal and neocortical penumbral regions, both CTSB and Iba-1 immunoreactivities showed marked increase compared to the corresponding contralateral brain regions (Fig. 2A-C, arrowheads and insets), but a decrease in the ischemic core (Fig. 2A-C, Star). Higher magnification revealed the elevated CTSB immunoreactivity was primarily localized in neuron-like structures (Fig. 2, D—F, arrows) and to a lesser degree in the extracellular space (Fig. 2, D—F, Stars). In contrast, CTSB was rarely observed in the Iba-1 immunopositive microglial cells in the penumbral regions at 24 h of reperfusion (Fig. 2, D—F, arrowheads).

To further confirm the predominant neuronal localization of CTSB, we double-labeled brain sections from sham-operated mice and mice subjected to 40 min of MCAO followed by 24 h of reperfusion with CTSB (red) and NeuN antibodies (Fig. 3). In the neocortical (Cx) and striatal (Stri) regions of sham-operated mice, the anti-CTSB antibody labeled the perinuclear region as small dots in NeuN-positive neurons (Fig. 3, A and C, arrow). In comparison to the sham (Fig. 3, A and C, red, arrow) or the contralateral regions (data not shown), the increases in size and intensity of CTSB-immunolabeled structures in NeuN-positive post-MCAO penumbral neurons were statistically significant (Fig. 3, B and D, red, arrow). Furthermore, compared to the sham (Fig. 3, A and C, red, arrow), CTSB-immunoreactivity was diffusely increased both within NeuN-positive post-MCAO penumbral neurons and the surrounding extracellular space (Fig. 3, B and D, red, arrow and arrowheads). The ratio of CTSB to NeuN (CTSB/NeuN) immunoreactivities in post-MCAO Cx and Stri neurons showed a statistically significant increase at 24 h of reperfusion, compared to that in the corresponding regions in sham-operated mice (Fig. 3E, $p < 0.05$), indicating the release of CTSB from the endolysosomal structures into the cytoplasm and nearby extracellular space at 24 h of reperfusion following MCAO.

3.3. Depletion of NSF in post-ischemic penumbral neurons

We double-labeled the same brain sections from mice subjected to 40 min of MCAO followed by 24 h of reperfusion as shown in Fig. 2 with mouse anti-CTSB (red) and rabbit anti-NSF (green) antibodies (Fig. 4). In the contralateral hemispheres, NSF immunoreactivity was observed in the perinuclear region (Fig. 4, A and C, green, arrows), while CTSB

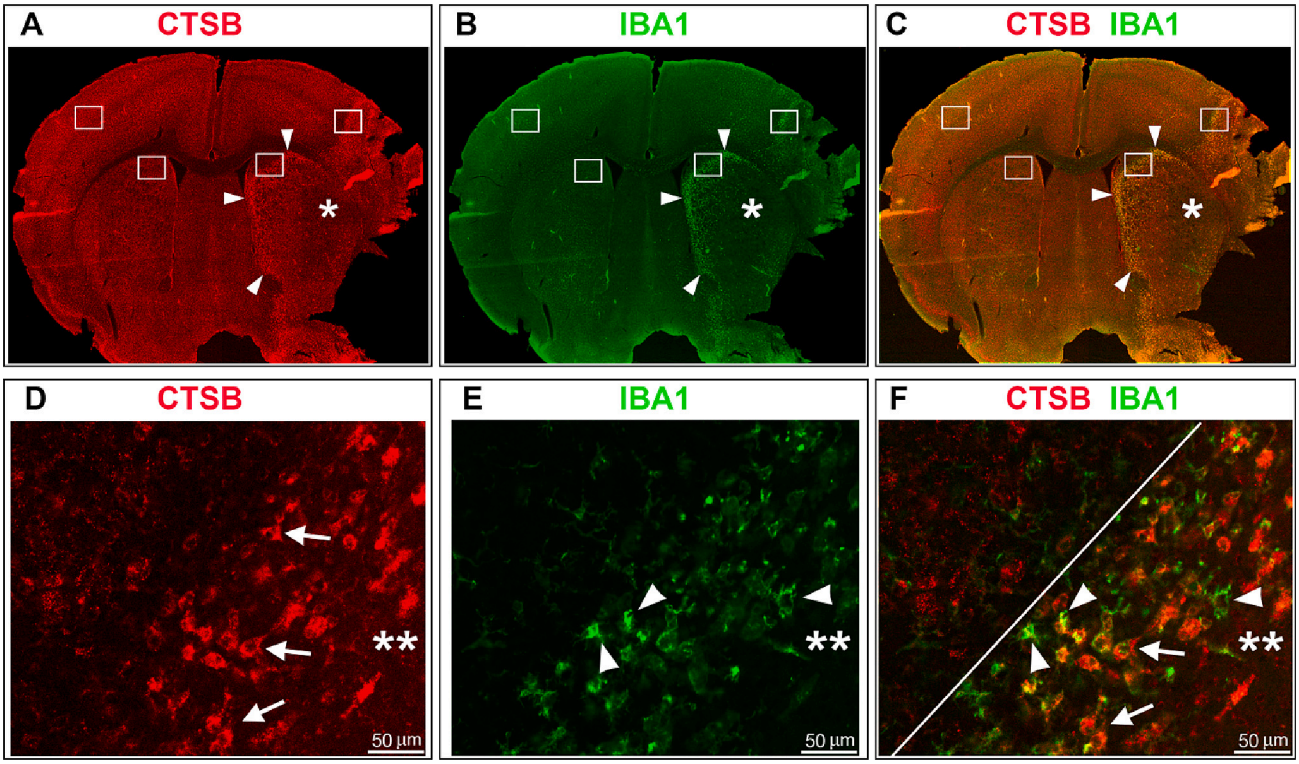

Fig. 2. *Buildup of CTSB primarily in post-MCAO neurons. A-C:* Confocal microscopic images of a brain section at the Bregma 1.30 mm level from a mouse subjected 40 min of MCAO followed by 24 h of reperfusion. Brain section was double-labeled with CTSB (red) and Iba-1 (green) antibodies. Arrowheads in *A-C* point to the striatal ischemic area. The insets represent the respective ipsilateral striatal and cortical "penumbral" and the corresponsive contralateral brain regions. Star indicates the ischemic core area. *D-F:* Higher magnifications of the cortical insets of *A-C*. Arrows point to CTSB immunolabeled neuronal structures. Arrowheads denote Iba-1 immunostained microglial cells. Stars indicate the extracellular space area. The white line separates the upper-left non-damaged area from the lower-right penumbral area. Scale bars = 50 μm. (For interpretation of the references to color in this figure legend, the reader is referred to the web version of this article.)

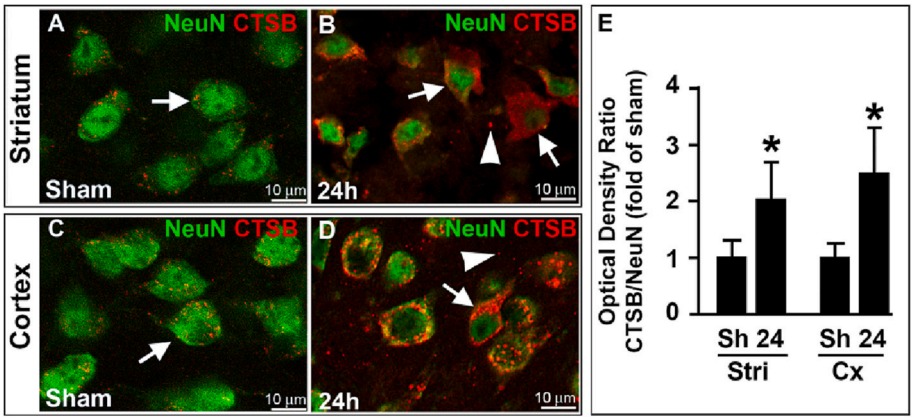

Fig. 3. *Confocal microscopy of endolysosomal structures. A-D:* Red and green channel merged confocal microscope images of respective striatal and cortical neurons of the corresponding "ipsilateral" inset areas of Fig. 2 (A-C) from mice subjected to sham-surgery (Sham) or 40 min of MCAO followed by 24 h of reperfusion (24 h). Brain sections were double-labeled with CTSB (red) and NeuN (green) antibodies. Arrows point to respective NeuN (green) and CTSB (red) co-immunolabeled sham and post-MCAO neurons. Arrowheads denote extracellular CTSB. Scale bars = 10 μm. *E:* Quantitative analysis of the ratio between CTSB (red color) and NeuN (green color) immunoreactivities in the striatum (Stri) and cortex (Cx) brain sections from sham-operated mice (Sh) and mice subjected to MCAO followed by 24 h reperfusion (24). Data are mean ± SEM ($n = 5$ per group, see Methods). *$p < 0.05$, two-tailed *t*-test. (For interpretation of the references to color in this figure legend, the reader is referred to the web version of this article.)

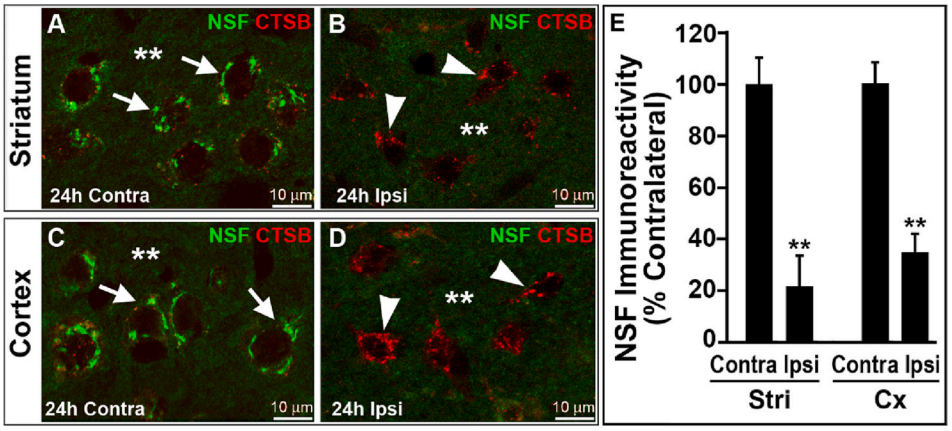

Fig. 4. *Depletion of N-ethylmaleimide sensitive ATPase (NSF) in post-MCAO neurons.* Confocal microscopic images of respective contralateral (Contra) and ipsilateral neurons of the corresponding striatal and cortical inset areas of Fig. 2 (A-C) from mice subjected to 40 min of MCAO followed by 24 h of reperfusion (24 h). Brain sections were double-labeled with CTSB (red) and NSF (green) antibodies. Arrows point to respective NSF (green) and CTSB (red) co-immunolabeled sham neurons. Arrowheads denote post-MCAO neurons with increased CTSB and depleted NSF immunoreactivities. Scale bars = 10 μm. *E:* Quantitative analysis of the level of NSF (green color) immunoreactivities in the striatal (Stri) and cortical (Cx) brain sections from the ipsilateral (Ipsi) and corresponding contralateral (Contra) brain regions. Data are mean ± SEM (n = 5 per group, see Methods). **$p < 0.01$, two-tailed t-test. (For interpretation of the references to color in this figure legend, the reader is referred to the web version of this article.)

labeling appeared as small dots in the same neurons (Fig. 4, A and C, red, arrows). Neurons were identified under confocal microscopy based on the round or conical-shaped soma or the presence of apical dendrites (Fig. 4, A and C, arrows). NSF immunoreactivity was also seen in the neuropil area, likely representing the presynaptic terminal NSF (Fig. 4, A and C, green, Stars) (Liu and Hu, 2004). The CTSB immunostaining pattern was virtually identical between sham neurons and neurons from the contralateral hemisphere after MCAO (Fig. 3A Sham vs. Fig. 4A Contra).

Similar to the results in Fig. 3, ipsilateral CTSB immunoreactivity was markedly increased in post-MCAO neurons (Fig. 4, B and D, red, arrowheads). In stark contrast, the ipsilateral NSF immunoreactivity was virtually depleted from the inside of the post-MCAO neurons (Fig. 4, B and D, green, arrowheads). The reduction of NSF immunoreactivity in the ipsilateral (Ipsi) post-MCAO neurons was statistically significant at 24 h of reperfusion compared to the corresponding contralateral (Contra) neurons (Fig. 4E, $p < 0.01$, ipsi vs. contra).

3.4. CTSB KO decreases stroke brain injury

The CTSB KO in mice was confirmed through genotyping, and the complete absence of CTSB band on Western blot (Supplemental Fig. 2) and immunoreactivity in the brain sections under confocal microscopy (data not shown). The 7-day mortality rate was about 18.8% in CTSB KO mice and 25.0% in wt mice, but the difference was not statistically significant (Supplemental Fig. 3). Brain sections at the striatal (−0.15 mm from Bregma) and hippocampal (−2.15 mm from Bregma) levels were stained with H&E, and the damaged area and the number of injured neurons were analyzed (Fig. 5). In this mouse MCAO model, 40 min of MCAO led to tissue injury in the core with few viable cells present at the striatal and nearby cortical regions, and selective neuronal damage in the hippocampal region, as shown in Fig. 5A. Fig. 5B shows that the damaged areas in the CTSB KO mice were almost significantly smaller statistically in the striatal plane (Fig. 5C, CTSB KO vs. wt, $p < 0.06$) and dramatically reduced in the hippocampal plane (Fig. 5D, CTSB KO vs. wt, $p < 0.01$) compared to the same damaged areas in wt mice after MCAO.

The striatal ischemic core area often contained surviving neurons after 40 min of MCAO followed by 7 days of reperfusion. To determine if there were more surviving neurons in the striatal damage areas in CTSB KO mice than in wt mice after MCAO, we quantified surviving neurons using an unbiased stereological method in the striatal ischemic core (Supplemental Fig. 4 and Fig. 5E). The number of surviving neurons per cubic millimeter volume in the ipsilateral striatal ischemic core after MCAO was significantly higher statistically in CTSB KO mice compared to wt mice (Fig. 5E, $33.16 +/- 3.76 \times 10^3$ vs. $14.88 +/- 1.75 \times 10^3$, $p < 0.01$). For reference, the contralateral striatal area contained $125.30 +/- 5.71 \times 10^3$ neurons in CTSB KO mice and $121.08 +/- 5.78 \times 10^3$

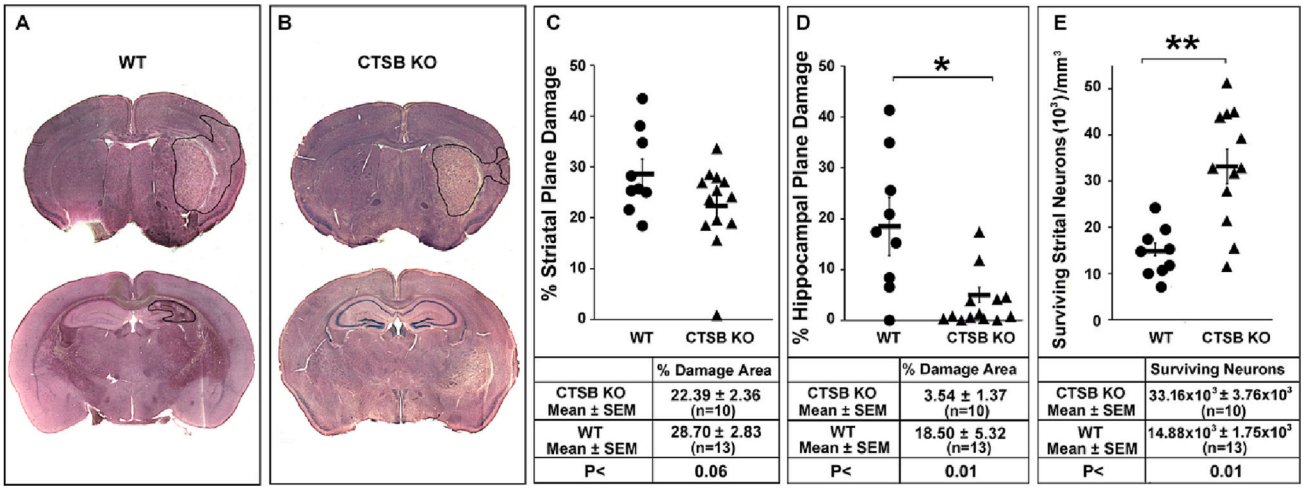

	% Damage Area
CTSB KO Mean ± SEM	22.39 ± 2.36 (n=10)
WT Mean ± SEM	28.70 ± 2.83 (n=13)
P<	0.06

	% Damage Area
CTSB KO Mean ± SEM	3.54 ± 1.37 (n=10)
WT Mean ± SEM	18.50 ± 5.32 (n=13)
P<	0.01

	Surviving Neurons
CTSB KO Mean ± SEM	$33.16x10^3 \pm 3.76x10^3$ (n=10)
WT Mean ± SEM	$14.88x10^3 \pm 1.75x10^3$ (n=13)
P<	0.01

Fig. 5. *Histopathological analysis of damaged areas and the number of damaged neurons after MCAO. A and B:* Representative coronal sections of mouse brains at the striatal (0.50 mm to Bregma) and hippocampal (−1.82 mm to Bregma) planes after MCAO. The borderline between the area containing only normal neurons and damaged tissue containing any recognizable damage neurons was delineated with a solid black outline. *C and D:* Average damage areas in the striatal and hippocampal planes from wt mice and CTSB KO mice subjected to 40 min of MCAO followed by 7 days of reperfusion. The percentage of ipsilateral damage area was calculated based on: undamaged contralateral area – undamaged ipsilateral area)/(undamaged contralateral area) x 100. Data shown as mean ± SEM. Data and *p*-values are indicated in the table. *E:* Average number of surviving neurons per cubic millimeter of volume in the striatal ischemic core. The surviving neurons within one cubic millimeter volume in the center of the striatal ischemic core were quantified using the SteroInvestigator program on a Zeiss AxioImager M2 Microscope Platform (MBF Biosciences, VA, USA) (Vereczki et al., 2006a). Data shown as mean ± SEM. Data and p-values are indicated in the table.

neurons per cubic millimeter in wt mice.

3.5. CTSB KO improves post-stroke physical and functional recovery

The nest-building activity is considered a measure of daily activity and well-being in mice (Yuan et al., 2018a). The surgical procedure and anesthesia can affect the nest-building activity, resulting in delayed nest-building even in sham-operated mice 1–2 days post-surgery (Yuan et al., 2018a). Two days post-surgery, both sham-operated mice and post-stroke CTSB KO mice resumed their nest-building activity, while most post-stroke wt mice showed a statistically significant reduction of nest-building activity (Fig. 6A). The nest-building activity was comparable between the post-MCAO CTSB KO mice and sham-operated non-ischemic mice, suggesting nearly full recovery of nest-building activity in CTSB KO mice after MCAO (Fig. 6A). In contrast, post-MCAO wt mice displayed significantly lower nest-building activity statistically from day 2 through day 7 of reperfusion compared to that of post-MCAO CTSB KO mice and sham-operated mice (Fig. 6A, CTSB KO vs. wt, $p < 0.01$).

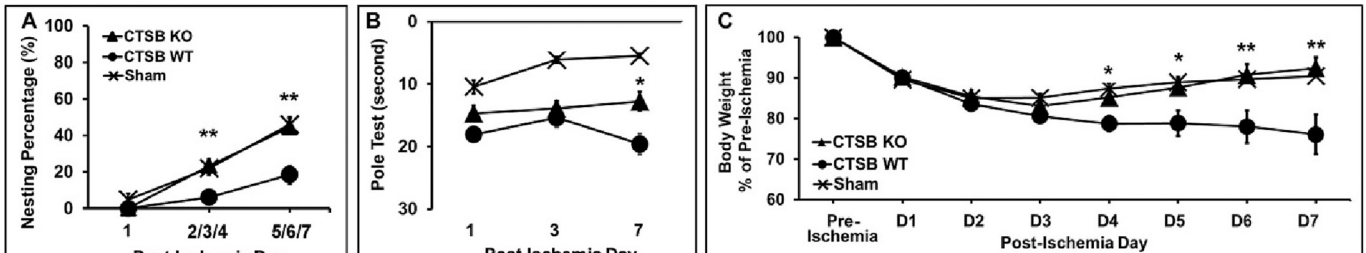

Post Ischemia Day	1	2/3/4	5/6/7
CTSB KO mean±SEM	0.00 ±0.00	23.36 ±3.80	44.52 ±4.54
CTSB WT mean±SEM	0.00 ±0.00	6.19 ±2.95	18.43 ±4.95
Sham mean±SEM	4.80 ±3.41	22.13 ±3.86	46.13 ±3.98
KO vs WT P<		0.01	0.01
KO vs Sham P<		1.00	1.00
WT vs Sham P<		0.02	0.01

Post Ischemia Day	1	3	7
CTSB KO mean±SEM	14.69 ±1.23	13.87 ±1.18	12.74 ±1.52
CTSB WT mean±SEM	18.06 ±1.22	15.38 ±1.48	19.57 ±1.65
Sham mean±SEM	10.45 ±1.10	6.10 ±0.50	5.45 ±0.34
KO vs WT P<	0.10	0.50	0.02
KO vs Sham P<	0.51	0.96	0.55
WT vs Sham P<	0.01	0.01	0.01

Time	Pre-Ischemia	Post-Ischemia Day 1	2	3	4	5	6	7
CTSB KO % mean±SEM	100.00 ±0.00	90.25 ±0.69	85.45 ±1.67	83.12 ±2.06	85.12 ±2.06	87.67 ±2.43	90.76 ±2.60	92.47 ±2.66
CTSB WT % mean±SEM	100.00 ±0.00	90.05 ±0.71	83.66 ±1.47	80.58 ±1.40	79.10 ±1.33	79.26 ±2.03	78.82 ±2.54	77.98 ±3.14
Sham % mean±SEM	100.00 ±0.00	89.58 ±1.09	85.05 ±0.94	85.10 ±0.99	87.47 ±1.13	88.94 ±1.27	89.72 ±1.14	90.48 ±0.86
KO vs WT P<		0.43	0.53	0.17	0.05	0.04	0.01	0.01
KO vs Sham P<		0.46	0.86	0.94	0.59	0.10	0.65	0.59
WT vs Sham P<		0.08	0.51	0.01	0.01	0.01	0.01	0.01

Fig. 6. Mouse nest-building activity (A), pole test (B), and body weight recovery (C) after MCAO. Mice were subjected to sham surgery or 40 min of MCAO followed by 7 days of reperfusion, respectively. Nest-building activity, pole test, and body weight were quantified in sham-operated mice, MCAO CTSB KO mice (CTSB KO, $n = 13$), MCAO wt mice (WT, $n = 8$), non-ischemic sham-operated CTSB KO mice (n = 8), and sham-operated wt mice (Sham, n = 8). There were no significant differences in these tests between sham-operated CTSB KO mice and sham-operated wt mice. For that reason, data from all sham-operated mice ($n = 16$) were combined in the analysis. *A:* Nest-building activity. *P* value of the day 1 (nest building activity) data in the table was left blank as the nest building activity was 0% in the CTSB KO and wt groups. *B:* Post-MCAO pole test performance. *C:* Post-MCAO body weight recovery. Body weight was calculated as percentage of the pre-ischemia body weight. Data shown in the tables below are mean ± SEM, $*p < 0.05$ and $**p < 0.01$, MCAO KO vs. MCAO WT, Wilcoxon-Mann-Whitney Test.

To assess forelimb strength, grip, and balance in mice, the vertical pole test was performed (Fig. 6B). Both post-MCAO CTSB KO and wt mice demonstrated poorer on the pole test performance compared to sham-operated non-ischemic mice. However, relative to sham control mice, only post-MCAO wt mice showed the statistically significant worse pole test performance (Fig. 6B, sham vs. wt MCAO, $p < 0.01$). Notably, CTSB KO mice exhibited significantly better pole test performance statistically relative to that of wt mice at 7-day reperfusion timepoint after MCAO (Fig. 6B, 7-day, CTSB KO MCAO vs. Wt MCAO, $p < 0.02$).

Body weight recovery is one of the most sensitive indicators of physical recovery in mouse stroke models (Lourbopoulos et al., 2017). Mice were weighed 5 min prior to the initiation of the MCAO procedure (pre-MCAO) and then weighed daily throughout the 7-day post-MCAO period. As shown in Fig. 6C, mouse body weights were consistently lower in the first 2 days post-surgery for both post-MCAO and sham-operated mice. However, body weight started recovering from post-surgery days 2–3 onwards and nearly reached the pre-MCAO level at post-MCAO day 7 in sham-operated mice (Fig. 6C). Post-MCAO CTSB KO mice had a similar degree of body weight recovery as that of sham-operated control mice (Fig. 6C). In contrast, the body weight of post-MCAO wt mice did not recover and continued to decline until the 7-day endpoint post-MCAO (Fig. 6C).

4. Discussion

This study presents several significant findings. First, there were statistically significant increases in the size and number of CTSB-labeled endolysosomal structures, leading to structural damage and subsequent release of CTSB into the cytoplasm and extracellular space from post-MCAO neurons. Second, CTSB KO in mice resulted in statistically significant histopathological, functional, and physical protection against stroke brain injury in the mouse model. These new findings suggest that the buildup and subsequent release of CTSB following ischemia contributes to cell death in stroke brain injury.

4.1. Rigor and reproducibility

The rodent intraluminal monofilament MCAO model is widely used in stroke research (Yuan et al., 2018a). However, a significant challenge arises due to a considerable variability in reported infarct volumes across published studies, with differences reaching up to approximately fivefold (Lourbopoulos et al., 2017; Carmichael, 2005; Barber et al., 2004). This inconsistency poses a significant challenge when utilizing the rodent intraluminal MCAO model to assess the efficacy of cerebroprotective interventions. Our own observation suggests that this inconsistency is attributed, at least in part, to the lack of control and confirmation of the extent of both ischemia and reperfusion during and following MCAO.

In the mouse intraluminal MCAO model, continuous monitoring of the MCA blood flow is crucial throughout the peri-MCAO period, to ensure the reproducibility of this model. The sharp drop of the MCA blood flow serves as an indication that the monofilament occluder has successfully occluded the MCA base (Yuan et al., 2018a). During the MCAO period, the MCA blood flow can surge even under anesthesia as shown Supplemental Fig. 5 (arrow). This surge is a result of the monofilament occluder moving away from the origin of the MCA during the MCAO period. When this surge is detected, the monofilament occluder needs to be adjusted, as shown by the arrow Supplemental Fig. 5. Without readjustment, the blood flow can return to 50% of the pre-ischemia level, leading to inconsistent ischemia.

There are also additional reasons why continuous MCA blood flow monitoring is crucial. Firstly, the pre-ischemic baseline level of the MCA blood flow signal recording can vary significantly among individual mice due to the exposed skull location and condition (e.g., degree of dryness or opaqueness). Therefore, changes in the blood flow signal during peri-MCAO periods are always relative to the pre-ischemic baseline level (Yuan et al., 2018a). Even a slight movement in positioning the laser doppler probe on the mouse skull surface can have substantial impact on the MCA blood flow recording signal (Yuan et al., 2018a). Secondly, it is essential to confirm reperfusion, as the post-stroke mice may have no or incomplete reperfusion after the removal of the monofilament occluder (Fig. 1). Ensuring consistent and reproducible animal modeling is paramount in brain protection studies, particularly when dealing with a limited number of animals per experimental group (about 10 mice).

The specificity of the CTSB and NSF antibodies used in this study has

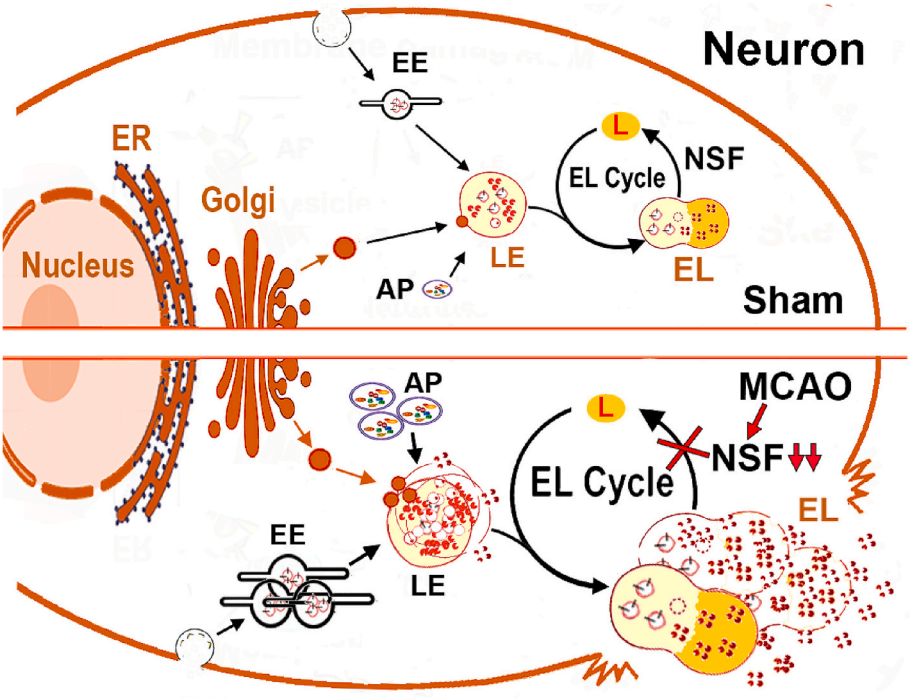

Fig. 7. *Schematic Post-Stroke CTSB Release. Upper:* In sham neurons, lysosomal hydrolytic enzymes and lysosomal structural proteins are synthesized on the ER-associated polyribosomes, modified in the ER and the Golgi lumen, and transported via vesicles to the late endosome (LE). The LE also receives incoming waste cargos from early endosome (EE) of the endocytic pathway and autophagosome (AP) of the autophagic pathway. The enzyme- and waste cargo-loaded LE then enters the "Endolysosomal Cycle" to fuses with an acidic terminal lysosome (L) for the formation of an endolysosome (EL) where the cargos can be degraded in an acidic environment (~pH 4.5). After degradation of waste cargos, EL converts into a new L via an NSF-mediated mechanism for the next round of LE-to-L fusion. *Lower:* MCAO leads to NSF deficiency in neurons, thus causing disruption of the EL's conversion to a new L. This results in the endocytic and autophagic traffic jams at the step of the EL's conversion to L. Consequently, both the size and number of all the structures related to the endocytic and autophagic pathways before the EL to L conversion phase, are increased. This cascade of events eventually damages the CTSB-containing structures to release CTSB into the cytoplasm or extracellular space contributing to stroke brain injury as seen in this study.

been extensively tested by Western blotting in our previous studies, demonstrating the presence of specific NSF and CTSB bands (Supplemental Fig. 2) (Yuan et al., 2021; Yuan et al., 2018c). We did not perform the Western blotting of CTSB in this study due to the heterogenicity of the brain injury within the focal brain ischemia brain subregions. As shown in Fig. 2, there is a significant increase in CTSB levels in the post-ischemic penumbral neurons adjacent to the non-ischemic tissue, while a notable decrease is observed in the ischemic core at 24 h of reperfusion after MCAO. The histopathological examinations in the consecutive brain sections confirmed that most penumbral neurons bordering with non-ischemic tissue maintained morphological integrity, exhibiting normal nuclear and cytoplasmic structures. This suggests that these neurons remained viable but were likely undergoing the cell death processes (Yuan et al., 2021; Yuan et al., 2018c). In comparison, the majority of the ischemic core neurons were already dead within the 24-h of reperfusion period after MCAO, as shown in Fig. 5. Due to the differential changes in CTSB expression between the ischemic core and penumbral subregions, as well as the difficulty associated with accurately dissecting the penumbral tissue for tissue lysates in Western blot analysis, confocal imaging was deemed a more suitable method for studying the level and distribution of CTSB after MCAO (Yuan et al., 2021; Yuan et al., 2018c).

4.2. Post-ischemic CTSB release from post-MCAO neurons

Under low magnification, Fig. 2C shows that CTSB immunostaining appeared to partially overlap or costain with Iba-1 immunostaining, resulting in a somewhat yellow color under confocal microscopy. This yellow color is likely because that some Iba-1 stained microglial cells were closely associated with the outer membranes of the penumbral neurons as seen at the higher magnification (Fig. 2F, arrowheads). Furthermore, at the higher magnification, CTSB immunostaining was mainly observed in neuron-like structures, and scantily distributed inside Iba-1 positive cells at 24-h post-MCAO (Fig. 2F). Moreover, our previous studies demonstrated that the increase in the CTSB level was minimal in GFAP-positive astrocytes at 24-h post-MCAO (Yuan et al., 2018c). This observation is consistent with findings from a recent study conducted on a separate murine model of a lysosomal disorder (Vereczki et al., 2006b). The double-immunostaining analysis confirmed the predominant distribution of CTSB in NeuN positive penumbral neurons at 24-h post-MCAO (Fig. 3). While CTSB is also a key lysosomal enzyme in phagocytes (e.g., microglia and macrophages) and astrocytes, the progressive activation of phagocytes and proliferation of astrocytes mainly occur after 24-h post-MCAO (Liu et al., 2009; Fifield and Vanderluit, 2020).

This study demonstrates a shift in the CTSB immunostaining pattern from small dots in the non-ischemic neurons to larger and more diffusely distributed spots in the cytoplasm and extracellular space surrounding post-MCAO neurons. Previous time course studies have shown that both increased CTSB and decreased NSF immunostaining pattern changes occur from 1-h reperfusion onward until neuronal death occurred after brain ischemia (Yuan et al., 2021; Yuan et al., 2018c). These observations suggest the presence of progressively accumulated CTSB structures and subsequent release of CTSB in post-ischemic neurons. Similar findings of intra-neuronal CTSB release have also been observed in a global ischemia model (Hu et al., 2021; Yuan et al., 2021; Yuan et al., 2018b). Fig. 7 illustrates our current understanding of the mechanism of CTSB release after brain ischemia. CTSB is synthesized in the ER, undergoes modification in the ER and Golgi lumens, and then transported from trans-Golgi-network to LE. The LE also receives waste cargo from both autophagic and endocytic pathways (Hu et al., 2021). In the LE, inactive forms of CTSB exists due to the high intraluminal pH (~pH 6.0). To degrade waste cargo, the LE must fuse with a more acidic compartment, forming an EL, where cathepsins become active (Hu et al., 2021). After degradation, the EL transforms into a new L through an NSF-dependent process (Fig. 7) for the next the endolysosomal cycle (Hu et al., 2021). The accumulation of larger CTSB-stained spots observed in post-MCAO neurons is likely attributed to the buildup of LE- and EL-related structures. This buildup occurs as a result of the slowing or complete stoppage EL to L conversion, which is caused by a depletion of active NSF (Fig. 4). Ultimately, this accumulation eventually leads to the release of CTSB into the cytoplasm and extracellular space (Fig. 7). Moreover, the disruption of the endolysosomal system after brain ischemia is likely to impede the degradation process of autophagic and endocytic structures, thereby affecting autophagic and endocytic flux. This disruption leads in the accumulation of endocytic and autophagic structures, such as early endosome (EE) and autophagosome (AP), as observed in previous studies, including our own (Fig. 7) (Hu et al., 2021; Yuan et al., 2021; Iwama et al., 2021).

4.3. CTSB KO protects brain tissue from MCAO

The endolysosomal structures contains at least 15 various cathepsins, with most exhibiting their highest activity in the acidic pH (~4.5) of these compartments. However, CTSB retains its endopeptidase activity at a neutral pH (Buck et al., 1992; Cavallo-Medved et al., 2011). Among the cathepsins implicated in cell death, CTSB and cathepsin D (CTSD) are commonly involved (Serrano-Puebla and Boya, 2016; Wouters and Bunt, 2016). CTSB is abundantly expressed in neurons (Petanceska et al., 1994), and CTSB-null mice did not have an obvious phenotype (Deussing et al., 1998; Felbor et al., 2002; Iwama et al., 2021). However, under pathological conditions, released CTSB from endolysosomal structures acts a major toxin to directly damage neurons and their surrounding tissue (Kingham and Pocock, 2001; Vidak et al., 2019).

Our study provides further evidence supporting the protective properties of CTSB KO in stroke brain injury in the mouse stroke model. CTSB KO mice demonstrated reduced brain damage areas, particularly in the hippocampal brain region, and a higher number of surviving neurons in the striatal ischemic core after MCAO (Fig. 5). Furthermore, CTSB KO mice exhibited significant recovery in the nest-building activity and body weight, as well as a moderate recovery in motor function in pole test (Fig. 3). Nest-building activity indicating an animal's overall well-being and working activity (Yuan et al., 2018a; Lin et al., 2007; Bachstetter et al., 2014). The recovery of body weight serves as a reliable indicator of physical recovery in the mouse MCAO model (Yuan et al., 2018a; Lourbopoulos et al., 2017).

4.4. Limitations of the study

Aging and sex are key bio-variables in stroke brain injury. The definition of sex in this study indicates female or male mice. This study used only young male mice. For that reason, the sex-based effect of CTSB KO on stroke brain injury remains to be studied. Furthermore, the systemic deletion of the CTSB gene in mice used in this study prevents us from conclusively determining whether the observed brain protection is specifically attributed to the absence of neuronal CTSB or the absence of CTSB in non-neuronal cells. Unfortunately, neuron-specific CTSB KO mice at the time of this study were not available. However, the accumulation and release of CTSB primarily occurred in post-MCAO neurons prior to the neuronal death, as observed in this study as well as our previous studies (Yuan et al., 2021; Yuan et al., 2018c). These studies suggests that the release of CTSB from post-MCAO neurons plays a role in brain injury after MCAO. Another limitation of this study is the potential unknown requirement of CTSB activity during the recovery phase after MCAO. Previous studies suggests that cathepsin L (CTSL) is capable of substituting the CTSB degradation function inside the endolysosomal lumen while having limited damaging activity in the neutral pH (~7.4) condition outside the endolysosomal lumen (Felbor et al., 2002). Therefore, further investigation into the role of CTSB and CTSL in the post-MCAO protection using inducible and cell-specific CTSB KO and CTSL KO mice is necessary.

Declaration of generative AI in scientific writing

None.

The authors have stated the sex definition and addressed the sex biovariable as a limitation to the research's generalizability in Discussion.

Sources of funding

This work was supported in part by National Institutes of Health (NIH) grants: NS097875, NS102815, NS129553, and NS130557 to BRH, as well as supported in part by Veteran Affair Merit grant: Award # BX005814 to BRH from the United States (U.S.) Department of Veterans Affairs Biomedical Laboratory Research and Development Service.

Disclaimer

The contents do not represent the views of the U.S. Department of Veterans Affairs or the United States Government.

Ethical approval

This article does not contain any studies with human subjects. All the experimental procedures involving the use of animals were approved by the Animal Use and Care Committee at the University of Maryland School of Medicine.

Declaration of Competing Interest

None.

Data availability

Data will be made available on request.

Acknowledgments

Kurt Hu, MD, Yujung Park, MD, and Chunli Liu, MD contributed to the study design, animal model, immunohistochemical analysis, data collection and interpretation, and writing of the manuscript. Yamileck Olivas MD, Chun Mun Loke, BS, Sungeong Lee, BS, and Jian Liang, MD, PhD contributed to the animal model and preparation of graphs. Bingren Hu, MD, PhD, designed the study and wrote the manuscript.

Appendix A. Supplementary data

Supplementary data to this article can be found online at https://doi.org/10.1016/j.expneurol.2023.114499.

References

Bachstetter, A.D., Webster, S.J., Tu, T., et al., 2014. Generation and Behavior Characterization of CaMKIIβ Knockout Mice. Skoulakis EMC, ed. PLoS One 9 (8). https://doi.org/10.1371/journal.pone.0105191 e105191.

Baker, R.W., Hughson, F.M., 2016. Chaperoning SNARE assembly and disassembly. Nat. Rev. Mol. Cell Biol. 17 (8), 465–479. https://doi.org/10.1038/nrm.2016.65.

Barber, P.A., Hoyte, L., Colbourne, F., Buchan, A.M., 2004. Temperature-regulated model of focal ischemia in the mouse: a study with histopathological and behavioral outcomes. Stroke. 35 (7), 1720–1725. https://doi.org/10.1161/01.STR.0000129653.22241.d7.

Bissig, C., Hurbain, I., Raposo, G., van Niel, G., 2017. PIKfyve activity regulates reformation of terminal storage lysosomes from endolysosomes. Traffic. 18 (11), 747–757. https://doi.org/10.1111/tra.12525.

Bright, N.A., Davis, L.J., Luzio, J.P., 2016. Endolysosomes are the principal intracellular sites of acid hydrolase activity. Curr. Biol. CB. 26 (17), 2233–2245. https://doi.org/10.1016/j.cub.2016.06.046.

Buck, M.R., Karustis, D.G., Day, N.A., Honn, K.V., Sloane, B.F., 1992. Degradation of extracellular-matrix proteins by human cathepsin B from normal and tumour tissues. Biochem. J. 282 (Pt 1), 273–278. https://doi.org/10.1042/bj2820273.

Carmichael, S.T., 2005. Rodent models of focal stroke: size, mechanism, and purpose. NeuroRx. 2 (3), 396–409.

Cavallo-Medved, D., Moin, K., Sloane, B., 2011. Cathepsin B: basis sequence: mouse. AFCS-Nat. Mol. Pages. 2011. A000508.

de Araujo, M.E.G., Liebscher, G., Hess, M.W., Huber, L.A., 2020. Lysosomal size matters. Traffic Cph Den. 21 (1), 60–75. https://doi.org/10.1111/tra.12714.

de Duve, C., 2005. The lysosome turns fifty. Nat. Cell Biol. 7 (9), 847–849. https://doi.org/10.1038/ncb0905-847.

Deussing, J., Roth, W., Saftig, P., Peters, C., Ploegh, H.L., Villadangos, J.A., 1998. Cathepsins B and D are dispensable for major histocompatibility complex class II-mediated antigen presentation. Proc. Natl. Acad. Sci. U. S. A. 95 (8), 4516–4521. https://doi.org/10.1073/pnas.95.8.4516.

Felbor, U., Kessler, B., Mothes, W., et al., 2002. Neuronal loss and brain atrophy in mice lacking cathepsins B and L. Proc. Natl. Acad. Sci. U. S. A. 99 (12), 7883–7888. https://doi.org/10.1073/pnas.112632299.

Fifield, K.E., Vanderluit, J.L., 2020. Rapid degeneration of neurons in the penumbra region following a small, focal ischemic stroke. Eur. J. Neurosci. 52 (4), 3196–3214. https://doi.org/10.1111/ejn.14678.

Hong, W., Lev, S., 2014. Tethering the assembly of SNARE complexes. Trends Cell Biol. 24 (1), 35–43. https://doi.org/10.1016/j.tcb.2013.09.006.

Hu, K., Gaire, B.P., Subedi, L., et al., 2021. Interruption of Endolysosomal trafficking after focal brain ischemia. Front. Mol. Neurosci. 14. Accessed May 27, 2023. https://doi.org/10.3389/fnmol.2021.719100.

Iwama, H., Mehanna, S., Imasaka, M., et al., 2021. Cathepsin B and D deficiency in the mouse pancreas induces impaired autophagy and chronic pancreatitis. Sci. Rep. 11, 6596. https://doi.org/10.1038/s41598-021-85898-9.

Kingham, P.J., Pocock, J.M., 2001. Microglial secreted cathepsin B induces neuronal apoptosis. J. Neurochem. 76 (5), 1475–1484. https://doi.org/10.1046/j.1471-4159.2001.00146.x.

Lin, L., Chen, G., Kuang, H., Wang, D., Tsien, J.Z., 2007. Neural encoding of the concept of nest in the mouse brain. Proc. Natl. Acad. Sci. 104 (14), 6066–6071. https://doi.org/10.1073/pnas.0701106104.

Liu, C., Hu, B., 2004. Alterations of N-ethylmaleimide-sensitive atpase following transient cerebral ischemia. Neuroscience. 128 (4), 767–774. https://doi.org/10.1016/j.neuroscience.2004.07.025.

Liu, F., Schafer, D.P., McCullough, L.D., 2009. TTC, fluoro-jade B and NeuN staining confirm evolving phases of infarction induced by middle cerebral artery occlusion. J. Neurosci. Methods 179 (1), 1–8. https://doi.org/10.1016/j.jneumeth.2008.12.028.

Lourbopoulos, A., Mamrak, U., Roth, S., et al., 2017. Inadequate food and water intake determine mortality following stroke in mice. J. Cereb. Blood Flow Metab. Off. J. Int. Soc. Cereb Blood Flow Metab 37 (6), 2084–2097. https://doi.org/10.1177/0271678X16660986.

Papadopoulos, C., Kravic, B., Meyer, H., 2020. Repair or Lysophagy: dealing with damaged lysosomes. J. Mol. Biol. 432 (1), 231–239. https://doi.org/10.1016/j.jmb.2019.08.010.

Petanceska, S., Burke, S., Watson, S.J., Devi, L., 1994. Differential distribution of messenger RNAs for cathepsins B, L and S in adult rat brain: an in situ hybridization study. Neuroscience. 59 (3), 729–738. https://doi.org/10.1016/0306-4522(94)90190-2.

Repnik, U., Česen, M.H., Turk, B., 2013. The Endolysosomal system in cell death and survival. Cold Spring Harb. Perspect. Biol. 5 (1), a008755 https://doi.org/10.1101/cshperspect.a008755.

Serrano-Puebla, A., Boya, P., 2016. Lysosomal membrane permeabilization in cell death: new evidence and implications for health and disease. Ann. N. Y. Acad. Sci. 1371 (1), 30–44. https://doi.org/10.1111/nyas.12966.

Vereczki, V., Martin, E., Rosenthal, R.E., Hof, P.R., Hoffman, G.E., Fiskum, G., 2006a. Normoxic resuscitation after cardiac arrest protects against hippocampal oxidative stress, metabolic dysfunction, and neuronal death. J. Cereb. Blood Flow Metab. 26, 821–835.

Vereczki, V., Martin, E., Rosenthal, R.E., Hof, P.R., Hoffman, G.E., Fiskum, G., 2006b. Normoxic resuscitation after cardiac arrest protects against hippocampal oxidative stress, metabolic dysfunction, and neuronal death. J. Cereb. Blood Flow Metab. 26, 821–835.

Vidak, E., Javoršek, U., Vizovišek, M., Turk, B., 2019. Cysteine Cathepsins and their extracellular roles: shaping the microenvironment. Cells. 8 (3), 264. https://doi.org/10.3390/cells8030264.

Wang, F., Gómez-Sintes, R., Boya, P., 2018. Lysosomal membrane permeabilization and cell death. Traffic Cph Den. 19 (12), 918–931. https://doi.org/10.1111/tra.12613.

Winckler, B., Faundez, V., Maday, S., Cai, Q., Guimas Almeida, C., Zhang, H., 2018. The Endolysosomal system and Proteostasis: from development to degeneration. J. Neurosci. 38 (44), 9364–9374. https://doi.org/10.1523/JNEUROSCI.1665-18.2018.

Wouters, F.S., Bunt, G., 2016. Cathepsin B pulls the emergency brake on cellular necrosis. Cell Death Dis. 7 (3) https://doi.org/10.1038/cddis.2016.76 e2170-e2170.

Yoon, T.Y., Munson, M., 2018. SNARE complex assembly and disassembly. Curr. Biol. CB. 28 (8), R397–R401. https://doi.org/10.1016/j.cub.2018.01.005.

Yuan, D., Liu, C., Wu, J., Hu, B., 2018a. Nest-building activity as a reproducible and long-term stroke deficit test in a mouse model of stroke. Brain Behav. 8 (6), e00993 https://doi.org/10.1002/brb3.993.

Yuan, D., Liu, C., Hu, B., 2018b. Dysfunction of membrane trafficking leads to ischemia-reperfusion injury after transient cerebral ischemia. Transl. Stroke Res. 9 (3), 215–222. https://doi.org/10.1007/s12975-017-0572-0.

Yuan, D., Liu, C., Wu, J., Hu, B., 2018c. Inactivation of NSF ATPase leads to Cathepsin B release after transient cerebral ischemia. Transl. Stroke Res. 9 (3), 201–213. https://doi.org/10.1007/s12975-017-0571-1.

Yuan, D., Hu, K., Loke, C.M., Teramoto, H., Liu, C., Hu, B., 2021. Interruption of endolysosomal trafficking leads to stroke brain injury. Exp. Neurol. 345, 113827 https://doi.org/10.1016/j.expneurol.2021.113827.